STOCHASTIC ANALYSIS OF WATER FLOW IN HETEROGENEOUS UNSATURATED SOILS UNDER TRANSIENT CONDITIONS

by

Marco Ferrante and T.-C. Jim Yeh

Department of Hydrology and Water Resources
The University of Arizona
Tucson, Arizona 85721

Technical Report

of

Department of Hydrology and Water Resources
The University of Arizona

HWR95-040
(September 8, 1995)

INTRODUCTION

A numerical model for the analysis of uncertainty propagation in flow through unsaturated soils is developed. This model is based on the first-order Taylor series expansion of the discretized Richards' equation, for one-dimensional flow. Soil hydrologic properties, the saturated hydraulic conductivity and the pore size distribution, are assumed to be stochastic processes in space. The surface boundary conditions are considered to be deterministic variable in time or stochastic time series. The purpose of this model is to examine the effect of uncertainty in boundary conditions and heterogeneity on the pressure head and flux variance profiles at various times.

Spectral analysis and Monte Carlo simulations were used to verify this numerical model for flow under both steady and transient conditions. Also, the model is used to investigate the sensitivity of the uncertainty in pressure head to the variability of the soil properties. The dependence of pressure head variance on the flow conditions (drying or wetting) and on the boundary condition at the surface (Dirichlet or a Neuman) is examined.

In addition, this model is applied to evaluate the uncertainty in the recharge estimate due to our incomplete knowledge of the heterogeneity and surface boundary flux. The mean and variance of the flux and of the cumulative discharge at the water table, at each time step, are calculated. The relationship between these statistics and the variability in soil properties and surface boundary flux is explored.

MATHEMATICAL FORMUALTIONS

Head Uncertainty

If the Richards' equation for flow through one-dimensional, variably saturated porous media is approximated by a fully implicit finite element scheme, it can be expressed in a matrix form:

$$P(h_k,p)h_k=Q(h_k,p)h_{k-1}+f(h_k,p,u) \qquad (1)$$

As the notation used throughout this paper, boldface capital letters indicate matrices and boldface lowercase letters indicate vectors. In (1) $\mathbf{h}_k$ is the ($nx1$) vector of the capillary pressure head at the time t_k at each of the n nodes; the subscript "k" denotes the time level; $\mathbf{p}$ is the (n x mn) vector of the m parameters used to define the soil hydraulic properties; $\mathbf{u}$ is the (lxl) boundary conditions vector; $\mathbf{P}$ is the matrix associated with weighted unsaturated hydraulic conductivity values and moisture capacity terms evaluated at $\mathbf{h}_k$ and $\mathbf{Q}$ is the matrix associated with the weighted moisture capacity term evaluated at $\mathbf{h}_k$, and the vector $\mathbf{f}$ is related to the boundary conditions and the gravity term (*Yeh and Khaleel, 1985*; *Protopapas and Bras, 1990*).

Using the Vetter "calculus" (*Vetter 1971*, *Vetter 1973*, *Dettinger and al. 1981*), expanding (1) in Taylor series around the mean up to the first order, and taking the expected value yield the mean equation:

$$P(\hat{h}_k,\hat{p})\hat{h}_k=Q(\hat{h}_k,\hat{p})\hat{h}_{k-1}+f(\hat{h}_k,\hat{p},\hat{u}) \qquad (2)$$

where ^ represents the mean of the variables and parameters. (2) is essentially the traditional deterministic approach, using the mean values for the parameters and the variables and it is exactly the mean equation of the first order analysis (*Dettinger et al. 1981*).

Subtracting (2) from the Taylor expansion results in the perturbation equation that can be written as:

$$h_k'=F_k h_{k-1}'+G_k p'+O_k u' \tag{3}$$

with:

$$\begin{aligned} E_k&=(D_{h_k}P)(I_n*h_k)+P-(D_{h_k}Q)(I_n*h_{k-1})-D_{h_k}f \\ F_k&=E_k^{-1}[-Q] \\ G_k&=E_k^{-1}[-(D_pP)(I_n*h_k)+(D_pQ)(I_n*h_{k-1})+D_pf] \\ O_k&=E_k^{-1}[(D_uf)] \end{aligned} \tag{4}$$

where primes denote the perturbations. In (4) D_xA is the derivative of the matrix A with respect to the transpose of the vector x. Using a recursive formulation (*Townley et al.*, 1985; *Protopaps and Bras*, 1990), (3) at any given time step becomes:

$$h_k'=A_k h_0'+B_k p'+C_k u' \tag{5}$$

with

$$A_k=F_k A_{k-1} \quad , \quad B_k=F_k B_{k-1}+G_k \quad , \quad C_k=F_k C_{k-1}+O_k \tag{6}$$

where $\mathbf{h_0}'$ is the uncertainty in the initial condition. If the porous medium is under a steady-state flow initially, $\mathbf{h_0}'$ can be derived as follows.

Under the steady-state condition, the mean flow equation is:

$$A(\hat{h}_s,\hat{p})\hat{h}_s=f(\hat{h}_s,\hat{p},\hat{u}) \tag{7}$$

and the perturbation equation is

$$h_s'=G_0p'+O_0u' \tag{8}$$

where

$$\begin{aligned} E_0&=(D_{h_s}A)(I_n*h_s)+A-D_{h_s}f \\ G_0&=E_0^{-1}[-(D_pA)(I_n*h_s)+D_pf] \\ O_0&=E_0^{-1}[(D_uf)] \end{aligned} \tag{9}$$

Substituting this expression in the (5), the $\mathbf{h_k}$ perturbation at any given time becomes:

$$h_k'=B_kp'+C_ku' \tag{10}$$

with

$$B_k=F_kB_{k-1}+G_k \quad , \quad C_k=F_kC_{k-1}+O_k \tag{11}$$

and

$$B_0=G_0 \quad , \quad C_0=O_0 \tag{12}$$

Using (10), the relationship between the head covariance matrix $\mathbf{R_{hh}}$ and the parameters and boundary

conditions covariance matrices, $\mathbf{R}_{pp}$ and $\mathbf{R}_{uu}$, respectively, can be defined as

$$R_{hh}=E[h_k'h_k'^T]=B_kR_{pp}B_k^T+C_kR_{uu}C_k^T \tag{13}$$

provided that the soil parameters and the boundary conditions are uncorrelated. The expected value is denoted by $E[]$. The cross- covariance matrices, for the head, the parameters and the boundary conditions, are given by:

$$\begin{aligned} R_{hp}&=E[h_k'p'^T] = B_kE[p'p'^T]+C_kE[u'p'^T] = B_kR_{pp} \\ R_{ph}&=R_{hp}^T \end{aligned} \tag{14}$$

and

$$\begin{aligned} R_{hu}&=E[h_k'u'^T] = G_kE[p'u'^T]+O_kE[up'^T] = O_kR_{uu} \\ R_{uh}&=R_{hu}^T \end{aligned} \tag{15}$$

These relationships utilize the symmetrical property of the $\mathbf{R}_{pp}$ matrix. Because of the (12), the covariance matrix for the initial steady-state condition is the same except k=0. The covariance boundary conditions matrix, $\mathbf{R}_{uu}$ in the one dimensional case is a two-by-two matrix with the variance of boundary condition on the diagonal and zero on the off-diagonal terms.

For mathematic simplicity, we chose Gardner's model for describing the unsaturated hydraulic property of soils. That is,

$$\log K(h)=\log K_s+\alpha h \qquad \theta=(\theta_s-\theta_r)*\exp(\alpha h)+\theta_r \tag{16}$$

where K_s is the saturated hydraulic conductivity, α is the pore-size distribution parameter, θ is the water content, θ_s is the saturated water content, and θ_r is the residual water content. If we consider α and $f = \ln k_s$ as stochastic processes, then

$$R_{pp} = \begin{bmatrix} R_{ff} & R_{f\alpha} \\ R_{\alpha f} & R_{\alpha\alpha} \end{bmatrix} \tag{17}$$

where R_{ff} and $R_{\alpha\alpha}$ are the covariance functions of lnKs and α, respectively. The cross-covariance is represented by $R_{\alpha f}$ and $R_{f\alpha}$. No field data sets are available for determining the cross-covariance between f and α. In this study, we assume a general relationship between the two parameters

$$f' = \xi^{-1}\alpha' + (1-\omega)f'_u$$

where ξ is the pressure head at the crossing point of the unsaturated hydraulic conductivity curve (*Yeh, 1987*) and ω is the cross correlation coefficient. The covariance matrix becomes:

$$R_{pp} = \begin{bmatrix} \omega^2\xi^{-2}R_{\alpha\alpha} + (1-\omega)^2 R_{f_u f_u} & \omega\xi^{-1}R_{\alpha\alpha} \\ \omega\xi^{-1}R_{\alpha\alpha} & R_{\alpha\alpha} \end{bmatrix} \tag{19}$$

For the cases of perfectly correlated and uncorrelated parameters, $\omega = 0$ and $\omega = 1$, respectively.

Flux Uncertainty

The finite element formulation of the Darcy's equation for the unsaturated flow yields

$$q=F(h_k,p,u) \tag{20}$$

The Taylor series expansion up to the first order of (19) gives:

$$q=F(\hat{h}_k,\hat{p},\hat{u})+(D_{h_k}F)(h_k-\hat{h}_k)+(D_p F)(p-\hat{p})+(D_u F)(u-\hat{u}) \tag{21}$$

The expected value of the flux is given by:

$$\hat{q}=F(\hat{h}_k,\hat{p},\hat{u}) \tag{22}$$

Therefore, the perturbation equation is:

$$q'=M_{h_k}h_k'+M_p p'+M_u u' \tag{23}$$

with:

$$M_{hk}=D_{h_k}F \quad , \quad M_{pk}=D_p F \quad , \quad M_{uk}=D_u F \tag{24}$$

or:

$$q'=V_k p'+Z_k u' \tag{25}$$

with:

$$V_k=M_{hk}B_k+M_{pk} \quad , \quad Z_k=M_{hk}C_k+M_{uk} \tag{26}$$

Using this formula is possible to evaluate the autocovariance matrix for the flux:

$$R_{qq}=E[q'q'^{T}] = M_{h_k}R_{hh}M_{h_k}^{T}+M_{h_k}R_{hp}M_{p}^{T}+M_{h_k}R_{hu}M_{u}^{T}+ \\ +M_{p}R_{ph}M_{h_k}^{T}+M_{p}R_{pp}M_{p}^{T}+M_{u}R_{uh}M_{h_k}^{T}+M_{u}R_{uu}M_{u}^{T} \quad (27)$$

The cumulative discharge at any node from t=0 to t_k can be evaluated by

$$Q_k=\sum_{i=0}^{k} q_i \Delta t \quad (28)$$

where the time step Δt is assumed constant. The first order expansion for this relationship again gives the mean equation:

$$\hat{Q}_k=\sum_{i=0}^{k} \hat{q}_i \Delta t \quad (29)$$

and the perturbation equation:

$$Q_k=\sum_{i=0}^{k} q_i \Delta t=(X_k p'+Y_k u') \Delta t \quad (30)$$

with:

$$X_k=\sum_{i=0}^{k} V_i \quad , \quad Y_k=\sum_{i=0}^{k} Z_i \quad (31)$$

Based on this formula, the covariance of the cumulative discharge at any node in the flow domain is

$$R_{QQ} = E[Q_k' Q_k'^T] = X_k R_{pp} X_k^T + Y_k R_{uu} Y_k^T \quad (32)$$

RESULTS

The accuracy of the first-order model was tested against the results of Monte Carlo simulations for flow in a one-dimensional, vertical soil profile under transient wetting and drying conditions. For this test, the total length of the one-dimensional simulation domain is 2000 cm and was divided in 250 elements of 8 cm each. The soil parameters lnKs and α were assumed to be second-order stationary Gaussian processes with the means of Ks equal to 10 cm/min and α equal to $0.1 cm^{-1}$, and the variance of lnKs and α are 0.1 and $10^{-2} cm^{-2}$, respectively. An exponential covariance function was assumed for both ln K_s and α with an integral scale of 100 cm. No uncertainty is assumed for the θ_s and θ_r parameters and they are set to 0.8 and 0.006 respectively.

The constant flux boundary condition at the top changed suddenly from the initial mean value q_a= 0.002 cm/min to q_b= 0.006 cm/min and from q_a = 0.006 cm/min to q_b = 0.002 cm/min for the wetting and drying scenarios, respectively. The variances of the prescribed flux boundary conditions were kept the same for the two different prescribed fluxes in both scenarios ($\sigma_q^2 = 10^{-7} cm^2/min^2$) . The bottom boundary condition was always specified as a constant head h_a= 0 cm (representing the water table).

For the Monte Carlo simulations, two thousand realizations of random lnKs and α fields were generated with the specified means and covariance functions. The random field generator is described in Yeh (1989). For each realization, the fluxes at the top of the soil profile, q_a and q_b, were randomly produced from a normal distribution with the previously defined means and variances.

The first-order model was also applied to the Maddock sandy loam (*Carvello et al., 1976*) and the Panoche silty clay loam (*Nielsen et al., 1973*) to investigate the uncertainty of flow in soils with distinct hydraulic properties. The same geometry and boundary conditions as in the previous case were used. The mean values of Ks and α are 2.89 cm/hr and 0.147 cm^{-1}, respectively, for the Maddock sandy loam while the variance of lnKs is 7.45 and the variance of α is 0.0076 cm^{-2}. For the Panoche silty clay loam, the mean of Ks and variance of lnKs are 5.78 cm/day and 2.48; the mean and variance of α are 0.0294 cm^{-1} and 6.7×10^{-5} cm^{-2}, respectively. The correlation scales for the two parameters were kept the same as in the previous case.

Pressure Head Variances

The mean head distributions, derived from the Monte Carlo simulations and the numerical model are illustrated in Figures 1a and b for the wetting and drying scenarios. Since the numerical solution of the mean flow equation is first-order, differences between the Monte Carlo and the numerical solutions are expected.

Figures 1c and d show the propagation of head variances for the wetting and drying cases, respectively. In both cases, the initial (t=0) and final (t≈220) steady-state head distributions are uniform for most of the depth. The head variances at these two steady states agree with the results from the spectral analysis with unit mean gradient assumption (*Yeh et al., 1985*; *Yeh 1987*). As expected, in the wetting case the head variance at t=0 is larger than that at t=220 since the initial mean pressure head is larger.

During the wetting process, the transition from one steady state to the other takes place only at the wetting front. Therefore, the head variances at locations where the wetting front passed are

expected to conform to final steady-state head variance. On the other hand, the head variances at locations before the wetting front remain equal to the head variance at t=0. The transient effect on the head variability is, then, reflected at the wetting front. Based on Figure 1c, the head variances at the locations of mean wetting front are less than that of the initial head variance during the early times (t=20). As the mean wetting front moves further downward (t=60 and more), they grow and become larger than the steady-state head variance at t=0. The variances of heads then decrease when the front reaches the capillary fringe, where effect of the water table boundary condition takes place. During the early time (e.g., t=20), the minimum head variance coincides with the center of the mean wetting front where the mean pressure head gradient is largest. After this initial period, the head variance at the center of the wetting front gradually changes to the maximum.

In contrast to the wetting case, the head variances at the drying front are always greater than those of the initial steady-state. Here, the maximum value of the head variance follows the center of the drying front where the mean pressure gradient is the strongest. Note that the sign of the mean gradient is opposite to that of the wetting case. Nevertheless, this maximum value decreases as the front moving downward. When the front reaches the capillary fringe, the maximum head variance decreases rapidly toward the final steady state value.

The above results suggest that the head variance during transient flow through unsaturated porous media is correlated to the mean pressure gradient. In addition, the differences in the behavior of the head variances between drying and wetting cases manifest the large scale hysteresis effect: the head variance under transient flow depends on wetting or drying. These findings are very similar to those by *Mantoglu and Gelhar* (1987). In contrast to their findings, our simulations indicate that the head variance during the drying case is greater than that in the wetting case.

In general, the head variances derived from the Monte Carlo simulation are in agreement with those from the numerical first-order approximations although some discrepancies exist. These discrepancies can be attributed to both the differences in the mean estimate of the front and approximate nature of the head variances in our numerical model. In both the wetting and drying cases, the location of the peak of head variance calculated from the MCS always lags behind that from our numerical solution. Such a difference is also reflected in the mean pressure head distribution as shown in Figures 1a and b. Further, our numerical model consistently overestimates the peak values of the head variance at the wetting/drying fronts.

Since our numerical uncertainty model is linear, it is possible to analyze the individual contribution of the uncertainty in ln K_s , α and the flux at the land surface to the head variance. Figure 2a shows the effect of variability in ln K_s on the head variance propagation during the wetting case. The impacts of variability in α and the boundary flux q are illustrated in Figures 2b and 2c, respectively. The sum of these variances leads to the combined effect of all these uncertainty on the head variance (Fig. 1b). According to this Figures, in this conditions, the uncertainty on the parameters K_s and α act in a different way. The ln Ks variance seems to be the major contributor to the peak head variance that moves along with the wetting front. As opposite the component of the head variance due to the uncertainty on α and q are bounded by the steady state initial and final values. Because this values are proportional to the square of the mean head and to the inverse of the mean α, the effect of σ_α on the total head variance is aspected to vary according to this parameters.

Figures 3a and 3b refer to the same case of Fig. 1a and b, but with a constant head top boundary condition. The constant head values, h_a and h_b, are evaluated for a unit gradient steady state distribution for the flux q_a and q_b of the previous cases. The variance of this values is assumed

to be zero and the head variance distributions of Fig. 3c and d respect this assumption. Such as Figure 3 for the constant flux top boundary conditions, Fig. 4 shows the effect of the uncertainty on each parameter on the total head variance for the constant head boundary condition variance. Main differences are in the zero head variance at the surface and in the behavior of the head variance component due to the σ_f. In this case there is no head variance decrease for early times, nor for the wetting neither for the drying conditions.

The effect of variability in α of Maddock sandy loam on the head variance in time during wetting is shown in Figure 5a. The head variance is normalized by

$$\frac{\sigma_\alpha^2 H^2 J^2 \lambda^2}{A\lambda(1 + A\lambda)}$$

where σ_α^2 is the variance of α; $\hat{h}$ is the mean capillary pressure head; J is the mean hydraulic gradient in space; λ is the correlation scale and A is the mean of α. The value of the normalized head variance in Figure 5a is always smaller than one except at the capillary fringe where the mean hydraulic gradient is not unity. In addition, the magnitude of the peak decreases with time and the location of the peak also coincides with the center of the mean wetting front.

Similarly, Figure 5b shows the effect of variation in lnKs on the head variance normalized with respect to

$$\frac{\sigma_f^2 J^2 \lambda^2}{A\lambda(1 + A\lambda)}$$

where σ_f^2 is the variance of lnKs. The normalized head variance in Figure 5b behaves similarly to non-normalized head variance in Figure 1c.

In contrast to the wetting case (Figure 5a), values of the normalized head variances in drying are always greater than one except at the locations where the mean hydraulic gradient is not unity (Figure 6a). Again, the magnitude of the peak decreases with time and the location of the peak also coincides with the center of the mean wetting front. The influence of the variation in lnKs in the drying case is illustrated in Figure 6b.

The impacts of variability in α and lnKs under different initial and final flux (q_a = 0.001 cm/hr and q_b = 1.0 cm/hr) boundary conditions are demonstrated in Figure 7a and b, respectively. For this case, the head variances are greater than those in Figures 3a and b, indicating the dependence of the normalized head variance on the difference between the initial and final steady-state mean capillary pressure head values. The increase in the effect of σ_f^2 on the normalized head variance is much greater than that of σ_α^2.

The results for Panoche silty clay loam for the same conditions as in the Maddock sandy loam are displayed in Figures 8 to 10. Comparing Figure 8b with Figure 5b (Maddock sandy loam), it is evident that the smaller value of A prolongs the period of time at which the peak head variance is less than one. The dependence of the normalized head variance on the difference between initial and final steady-state mean pressure values is illustrated in Figures 9 and 10. The behavior is similar to that in the Maddock sandy loam.

Flux Variance

Figures 11 a and b show the comparison of the means and variances of flux at different times,

derived from the numerical model and the MCS (dotted lines). Again, the agreement is satisfactory with some discrepancies which can be attributed to the approximate nature of the first-order analysis. The peak variance in flux also follows the center of the mean wetting front. It grows continuously as the wetting front moving toward the water table without being affected by the water table boundary condition. Another finding is that the variance of the flux does not depend on the flow conditions, i.e., they are the same for both the wetting and drying cases.

Figures 5 to 10, c and d, show the results of flux variance analysis for the Maddock sandy loam and Panoche silty clay loam. The behaviors of the mean and variance of the fluxes are very similar to those described previously.

CONCLUSIONS

A first-order numerical model for the stochastic analysis of transient flow through variably saturated soils is developed. This model is capable of investigating the effect of heterogeneity on flow under realistic conditions such as bounded domains, uncertainty in boundary and initial conditions, and nonstationary processes. More importantly, it allows us to examine many cases which are excluded by the previously developed analytical/spectral method (e.g., *Mantoglou and Gelhar, 1987*). The model has been verified against the result of Monte Carlo simulation. In general, the behaviors of the evolution of the head and flux variances derived from the numerical model are in excellent agreement with those obtained from Monte Carlo simulation.

Based on our preliminary analysis, we found that boundary conditions (prescribed head or flux condition at the soil surface) have significant impact on the evolution of the head and flux variances. In addition, the head and flux variances are strongly correlated to the magnitude of the mean pressure gradient in space at the center of the wetting or drying front. The peak values of the variances always follow the wetting or drying front. The variability in lnKs and α produce different effects on the overall behavior of the head and flux variances. The adimensional analysis of the contribution from the variation in lnKs and α indicates a large-scale hysteresis effect on the head variance. The head variance in the case of drying is found to be much larger than that in the case of wetting. This result is different from those findings reported by *Mantoglou and Gelhar (1987)*. Furthermore, the variability in lnKs seems to play a more important role than the variability of α in this hysteresis phenomenon.

The model developed here can be applied to estimate the uncertainty in recharge estimates. The infiltration rate of moisture through the vadose zone (aquifer recharge) is probably the most important hydrologic variable that needs to be considered in the assessment of potential risk of groundwater contamination from ground surface spills or land management of wastes. Current methods for estimating ground water recharge involve large uncertainties and tend to overestimate moisture and water-borne contaminant infiltration rates. This has lead to extremely conservative approaches towards waste management regulation, site remediation and closure that are unnecessarily costly. Our first-order uncertainty model can be utilized as a method to assess the uncertainty in recharge estimates and thus, the contaminant infiltration rates, caused by our incomplete knowledge of hydrological heterogeneity and uncertainties in precipitation and evapotranspiration rates. It is our belief that this model is a valuable tool for water resources quality management.

REFERENCES

Carvello H. O., D. K. Cassel, J. Hammond, and A. Bauer, Spatial variability of in situ unsaturated hydraulic conductivity of Maddock sandy loam. *Soil Sci.*, 121(1), 1-8, 1976

Dettinger M. D. and J. L. Wilson, First order analysis of uncertainty in numerical models of groundwater flow, 1, Mathematical development, *Water Resour. Res.*, 17(1), 149-161, 1981.

Kabala Z. J. and P. C. D. Milly, Sensitivity analysis of flow in unsaturated heterogeneous porous media: theory, numerical model and its verivication, *Water Resour. Res.*, 26(4), 593-610, 1990

Mantoglu A. and L. W. Gelhar, Capillary tension head variance, mean soil moisture content, and effective specific soil moisture capacity of transient unsaturated flow in stratified soils, *Water Resour. Res.*, 23(1), 47-56, 1987 *a*

Mantoglu A. and L. W. Gelhar, Effective hydraulic conductivities for transient unsaturated flow in stratified soils, *Water Resour. Res.*, 23(1), 57-67, 1987 *b*

Nielsen, D. R., J. W. Biggar, and K. T. Erh, Spatial varaibility of field measured soil-water properties, *Hilgardia* 42(7), 215-260, 1973

Protopapas A. L. and R. L. Bras, Uncertainty propagation with numerica models for flow and transport in the unsaturated zone, *Water Resour. Res.* 26(10), 2463-2474, 1990

Srivastava R. and T. -C. J. Yeh, Analytical solutions for One dimensional , transient infiltration toward the water table in homogeneus and layered soils, *Water Resour. Res.*, 27(5), 753-762, 1991

Townley, L. R. and J. L. Wilson, Computationally efficient algorithms for parameter estimation and uncetainty propagation in numerical models of groundwater flow, *Water Resour. Res.*, 21(12), 1851-1860, 1985

Unlu K., D.R. Nielsen and J. W. Biggar, Stochastic analysis of unsaturated flow: one-dimensional Monte Carlo simulations and comparisons with spectral perturbation analysis and field oservations, *Water Resour. Res.*, 26(9), 2207-2218, 1990

Vetter W. J., Derivative operations on matrices, *IEE Trans. Autom. Control*, AC-15, 241-244, 1970

Vetter W. J., Correction to: Derivative operations on matrices, *IEE Trans. Autom. Control*, AC-16, 113, 1971

Vetter W. J., Matrix calculus operations and Taylor expansions, *SIAM Rev.*, 15(2), 352-369, 1973

Yeh T. -C. J., One-dimensional steady state infiltration in heterogeneous soils, *Water Resour. Res.*, 25(10), 2149-2158, 1989

Yeh T. -C. J., L. W. Gelhar and A. L. Gutjahr, Stochastic Analysis of unsaturated flow, 1, Heterogeneous soils, *Water Resour. Res.*, 21(4), 447-456, 1985 *a*

Yeh T. -C. J., L. W. Gelhar and A. L. Gutjahr, Stochastic Analysis of unsaturated flow, 2, Statistically anysotropic media with variable α, *Water Resour. Res.*, 21(4), 457-464, 1985 *b*

Yeh T. -C. J., L. W. Gelhar and A. L. Gutjahr, Stochastic Analysis of unsaturated flow, 3, Observation and applications, *Water Resour. Res.*, 21(4), 465-471, 1985 *c*

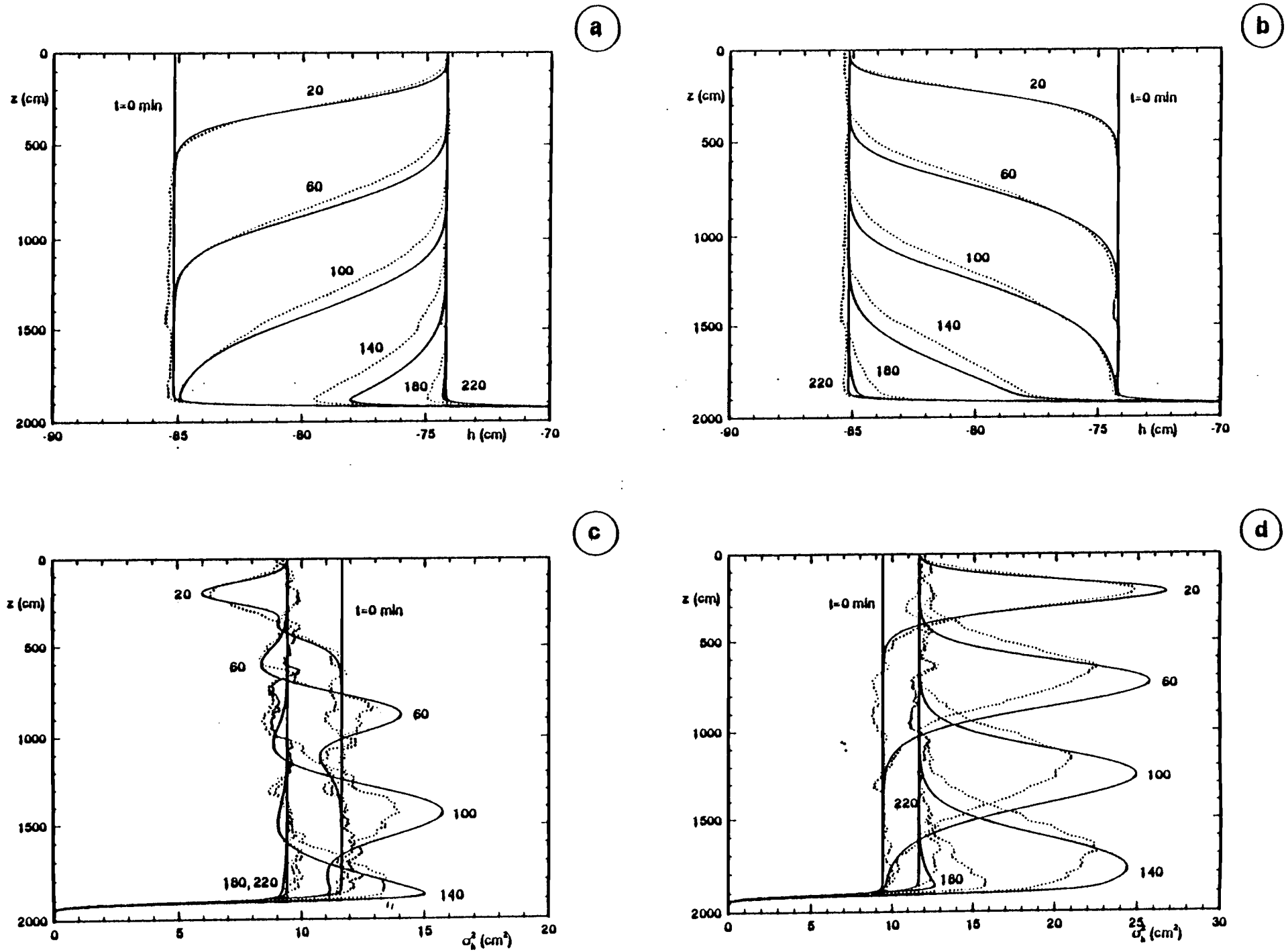
a
b
c
d
z (cm)
h (cm)
t=0 min
20
60
100
140
180
220
180, 220
0
500
1000
1500
2000
-90
-85
-80
-75
-70
5
10
15
20
25
30
σ_h^2 (cm^2)

Figure 1

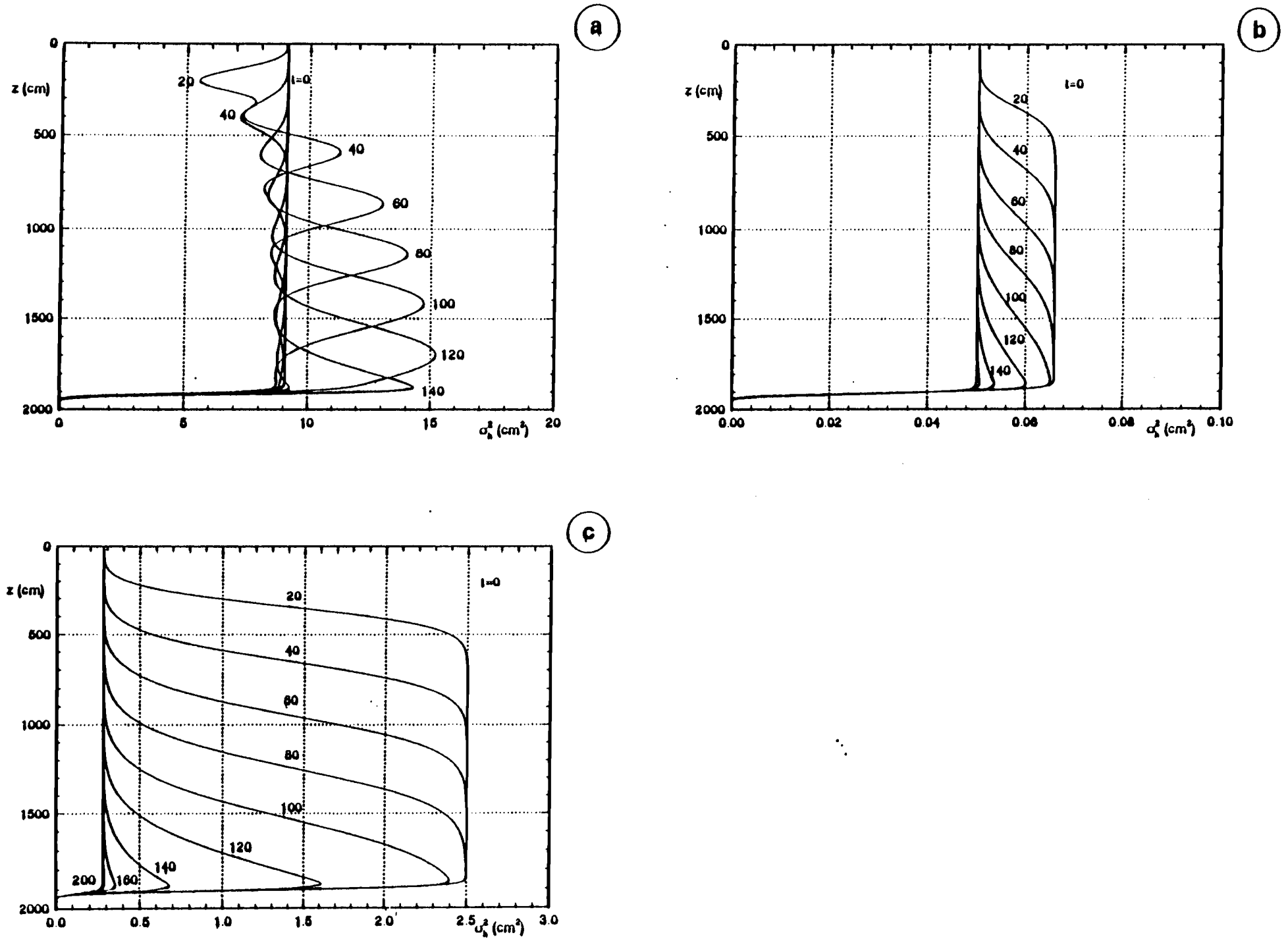
a
z (cm)
0
500
1000
1500
2000
t=0
20
40
40
60
80
100
120
140
0
5
10
15
20
σ_h^2 (cm^2)
b
z (cm)
t=0
20
40
60
80
100
120
140
0.00
0.02
0.04
0.06
0.08
0.10
σ_h^2 (cm^2)
c
z (cm)
t=0
20
40
80
80
100
120
140
160
200
0.0
0.5
1.0
1.5
2.0
2.5
3.0
σ_h^2 (cm^2)

Figure 2

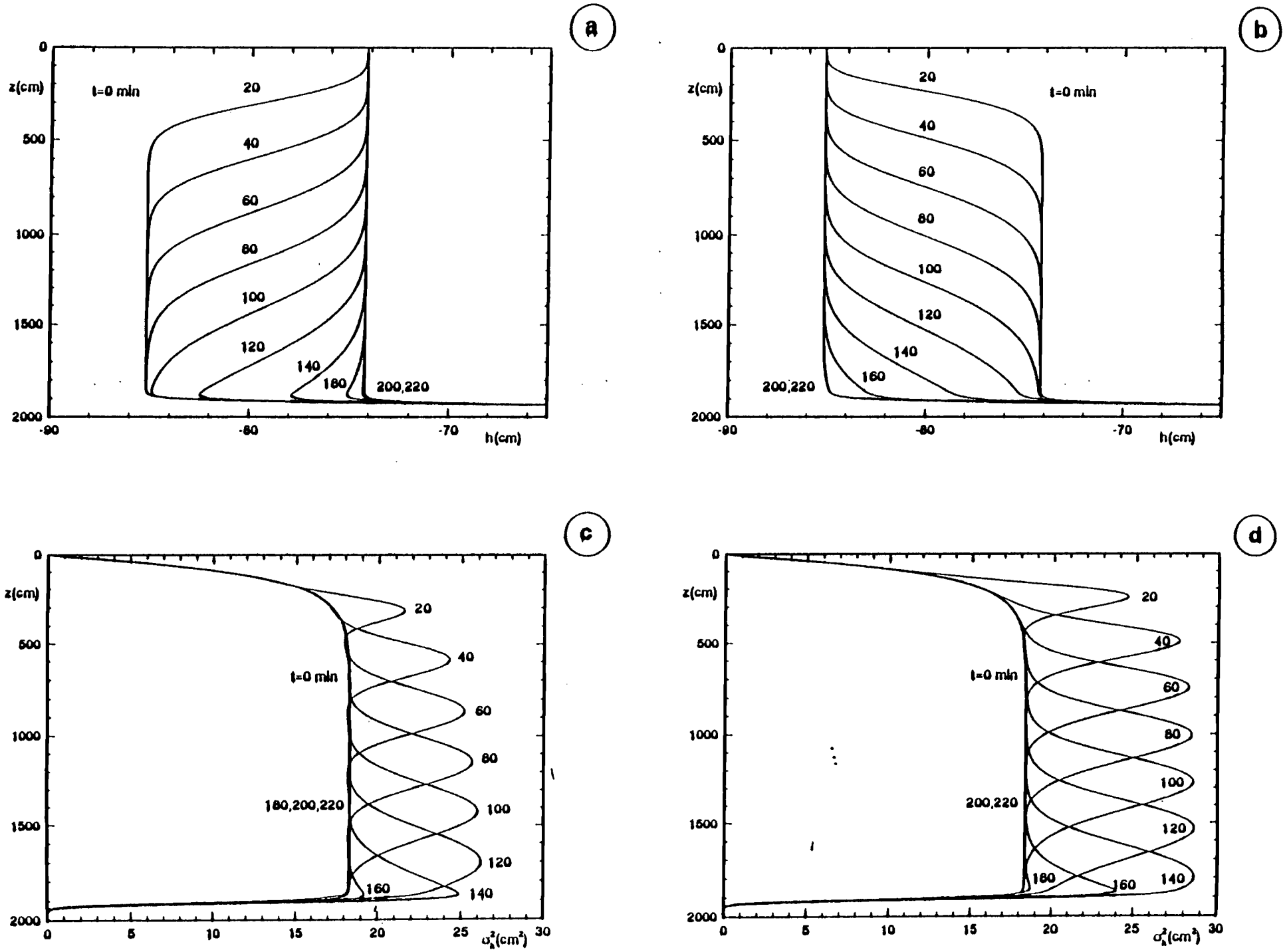
a
z(cm)
t=0 min
20
40
60
80
100
120
140
160
200,220
h(cm)
b
z(cm)
20
t=0 min
40
60
80
100
120
140
160
200,220
h(cm)
c
z(cm)
20
40
t=0 min
60
80
180,200,220
100
120
160
140
$\omega_h^2(cm^2)$
d
z(cm)
20
40
t=0 min
60
80
100
200,220
120
180
160
140
$\omega_h^2(cm^2)$

Figure 3

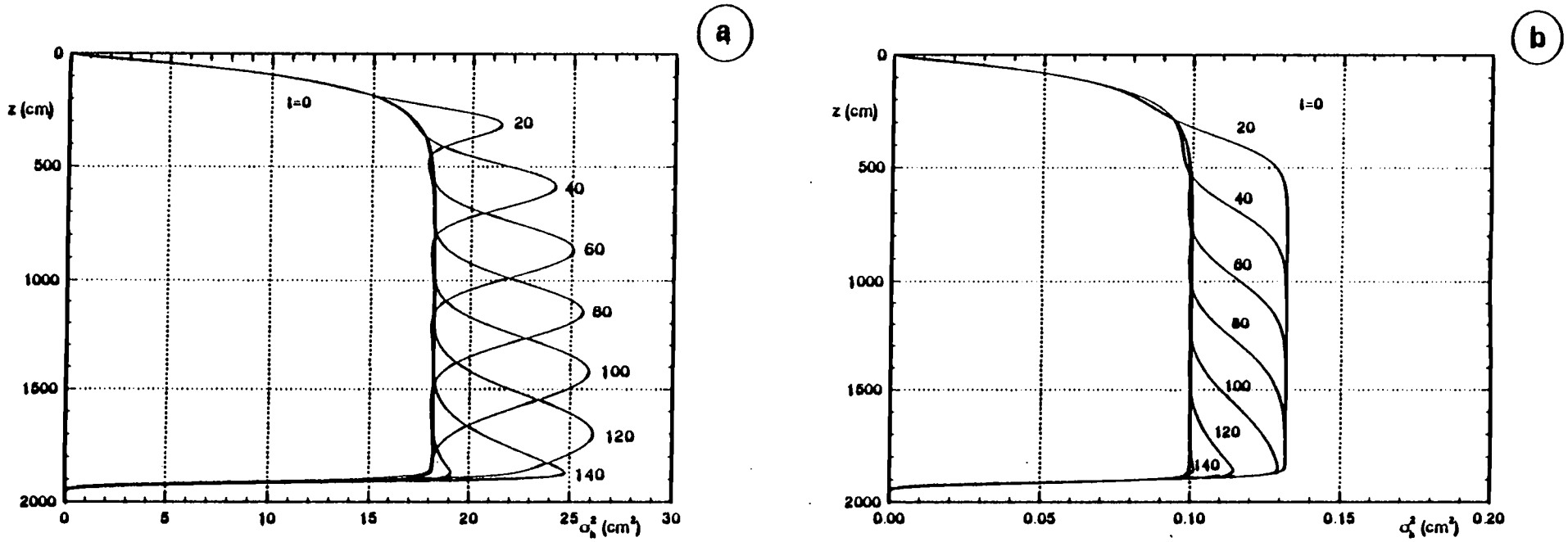
a
b
z (cm)
t=0
20
40
60
80
100
120
140
0
500
1000
1500
2000
0
5
10
15
20
25
30
0.00
0.05
0.10
0.15
0.20
σ_θ^2 (cm^3)

Figure 4

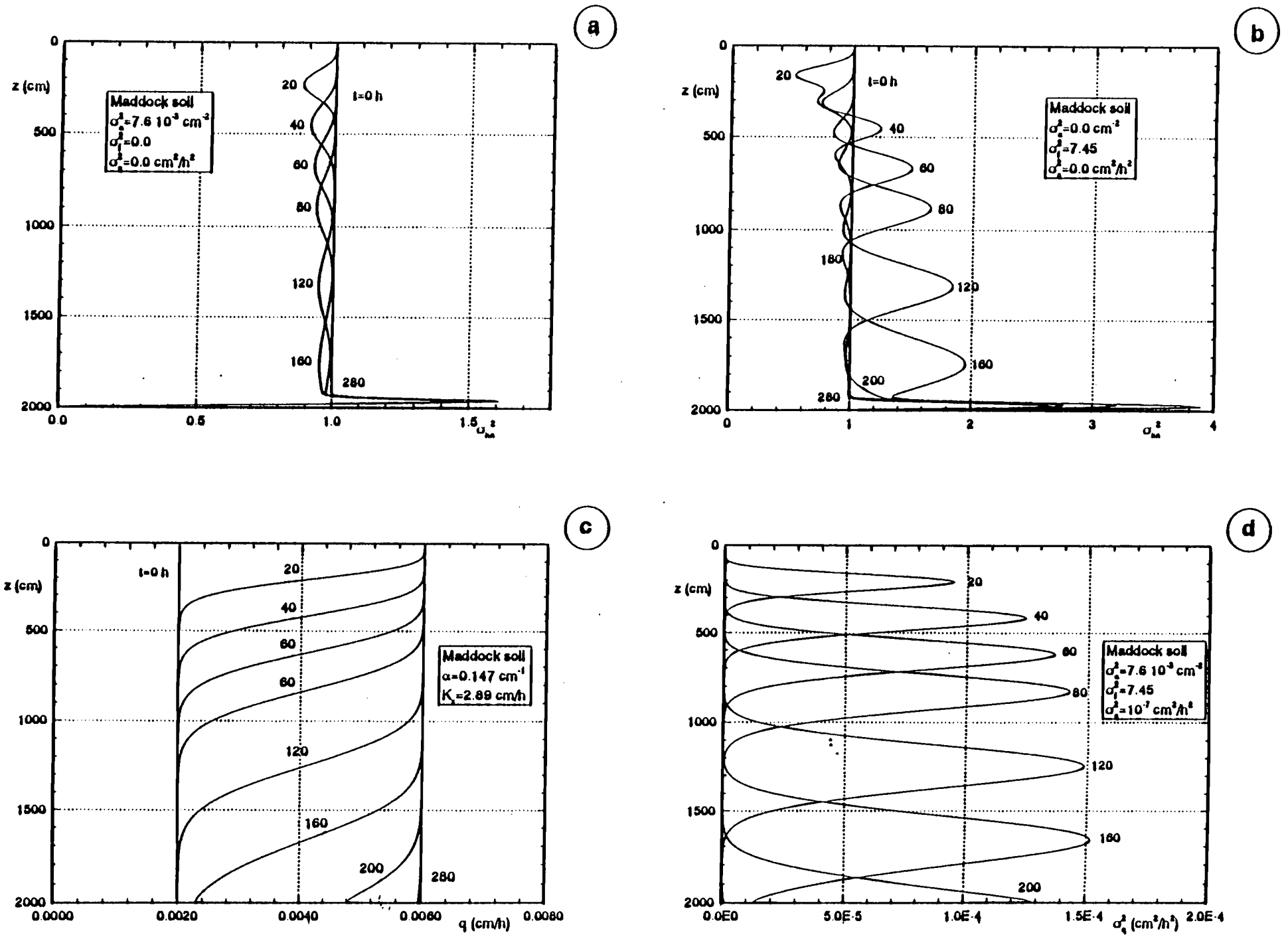
a
z (cm)
Maddock soil
σ_s^2=7.6 10^{-5} cm^{-2}
σ_q^2=0.0
σ_a^2=0.0 cm^2/h^2
t=0 h
20
40
60
80
120
160
280
σ_{hh}^2
b
z (cm)
t=0 h
20
40
60
80
180
120
160
200
280
Maddock soil
σ_s^2=0.0 cm^{-2}
σ_q^2=7.45
σ_a^2=0.0 cm^2/h^2
σ_{hh}^2
c
z (cm)
t=0 h
20
40
60
60
120
160
200
280
Maddock soil
α=0.147 cm^{-1}
K_s=2.89 cm/h
q (cm/h)
d
z (cm)
20
40
60
80
120
160
200
Maddock soil
σ_s^2=7.6 10^{-5} cm^{-2}
σ_q^2=7.45
σ_a^2=10^{-7} cm^2/h^2
σ_q^2 (cm^2/h^2)

Figure 5

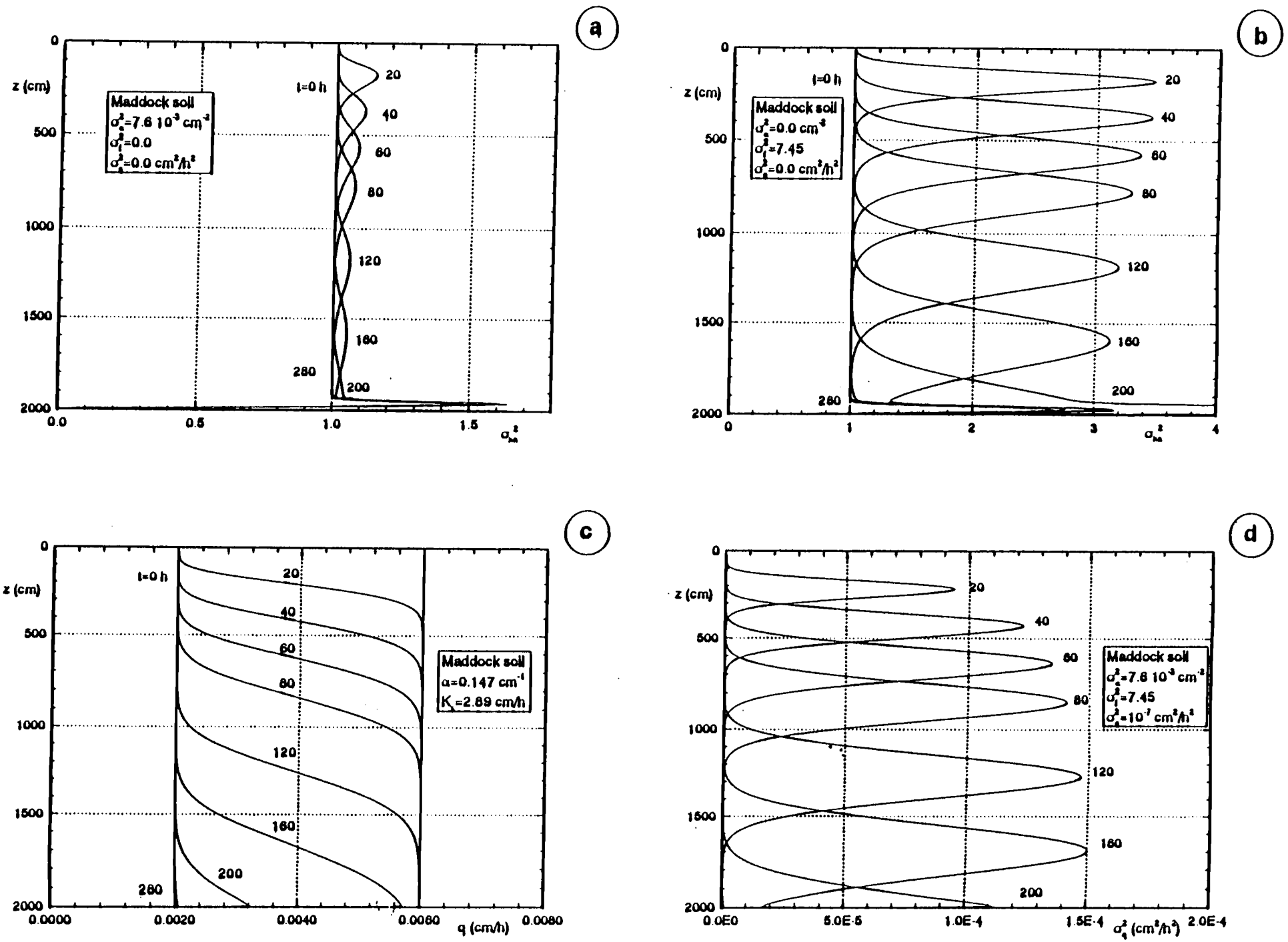
a
z (cm)
Maddock soil
σ_s^2=7.6 10^{-3} cm^{-2}
σ_I^2=0.0
σ_q^2=0.0 cm^2/h^2
t=0 h
20
40
60
80
120
160
200
280
σ_{hh}^2
b
z (cm)
Maddock soil
σ_s^2=0.0 cm^{-2}
σ_I^2=7.45
σ_q^2=0.0 cm^2/h^2
t=0 h
20
40
60
80
120
160
200
280
σ_{hh}^2
c
z (cm)
t=0 h
Maddock soil
α=0.147 cm^{-1}
K_s=2.89 cm/h
q (cm/h)
d
z (cm)
Maddock soil
σ_s^2=7.6 10^{-3} cm^{-2}
σ_I^2=7.45
σ_q^2=10^{-7} cm^2/h^2
σ_q^2 (cm^2/h^2)

Figure 6

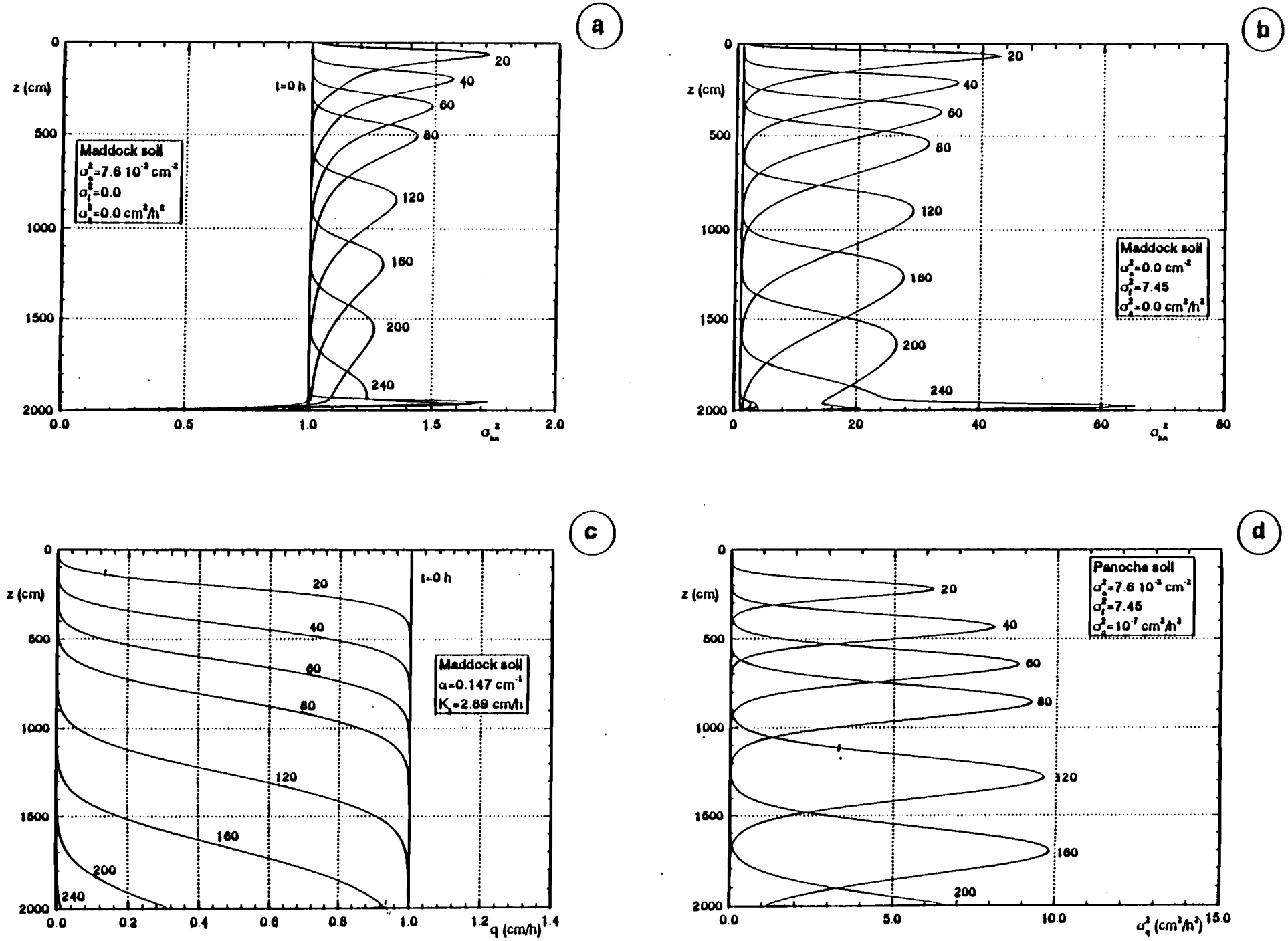
a
z (cm)
t=0 h
20
40
60
80
120
160
200
240
Maddock soil
σ_s^2=7.6 10^{-3} cm^{-2}
σ_f^2=0.0
σ_q^2=0.0 cm^2/h^2
σ_{hh}^2
b
Maddock soil
σ_s^2=0.0 cm^{-2}
σ_f^2=7.45
σ_q^2=0.0 cm^2/h^2
c
t=0 h
Maddock soil
α=0.147 cm^{-1}
K_s=2.89 cm/h
q (cm/h)
d
Panoche soil
σ_s^2=7.6 10^{-3} cm^{-2}
σ_f^2=7.45
σ_q^2=10^{-7} cm^2/h^2
σ_q^2 (cm^2/h^2)

Figure 7

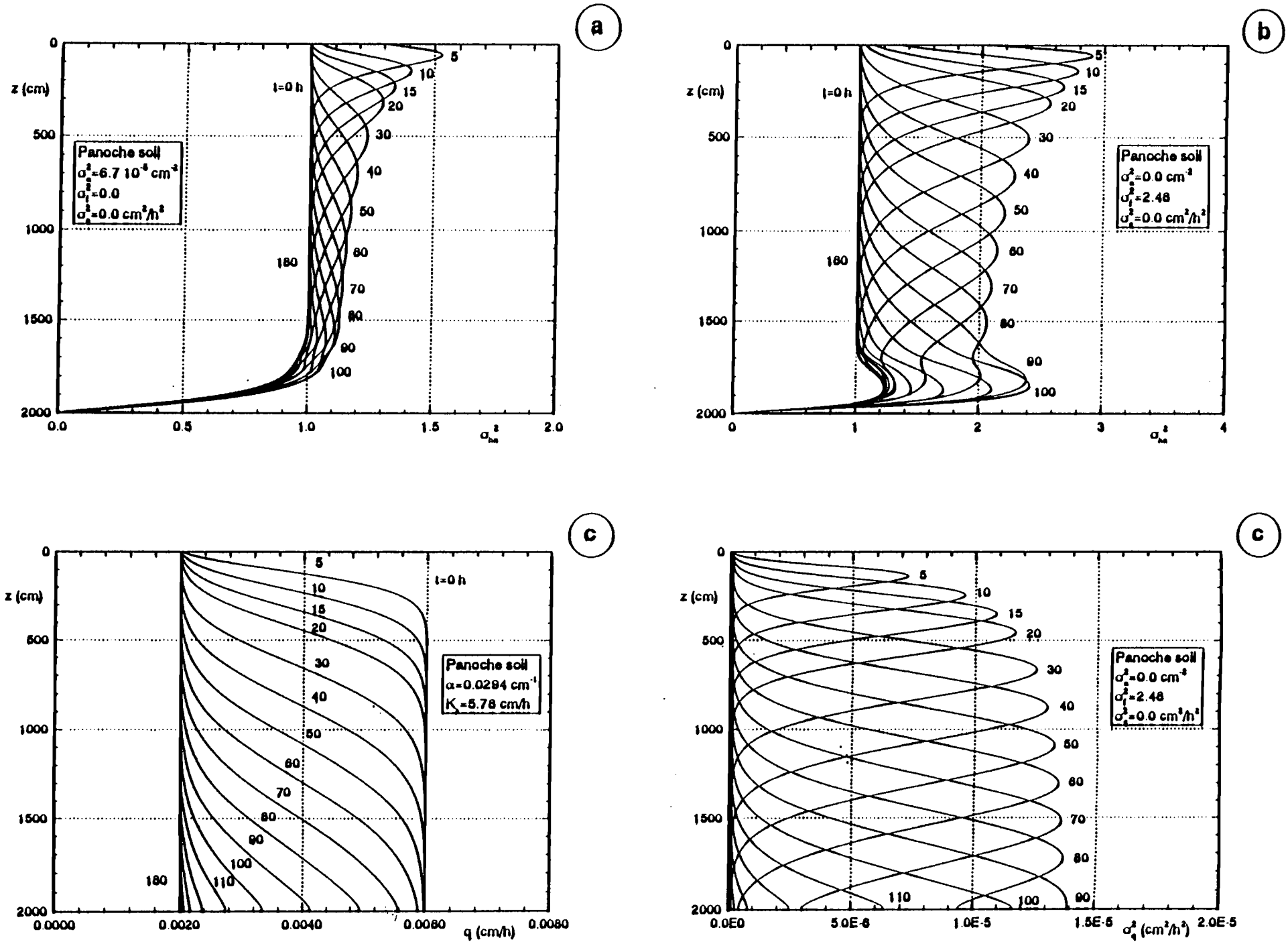
a
z (cm)
t=0 h
Panoche soil
σ^2_{hh}=6.7 10^{-5} cm^{-2}
σ^2_{hf}=0.0
σ^2_{hq}=0.0 cm^2/h^2
σ^2_{hh}
b
Panoche soil
σ^2_{hh}=0.0 cm^{-2}
σ^2_{hf}=2.48
σ^2_{hq}=0.0 cm^2/h^2
c
Panoche soil
α=0.0294 cm^{-1}
K_s=5.78 cm/h
q (cm/h)
c
Panoche soil
σ^2_{hh}=0.0 cm^{-2}
σ^2_{hf}=2.48
σ^2_{hq}=0.0 cm^2/h^2
σ^2_q (cm^2/h^2)

Figure 8

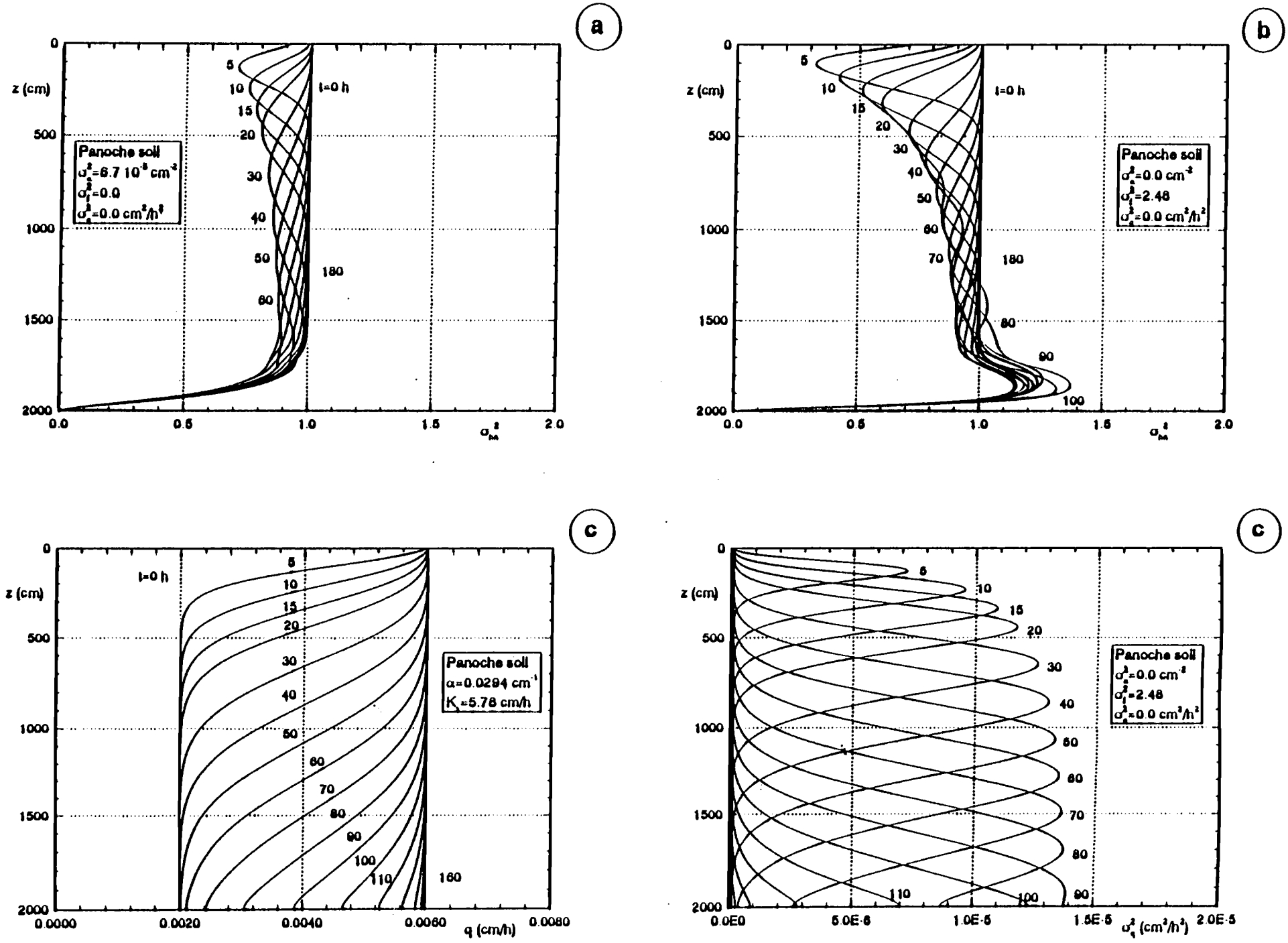
a
z (cm)
t=0 h
Panoche soil
σ_a^2=6.7 10^{-5} cm^{-2}
σ_f^2=0.0
σ_q^2=0.0 cm^2/h^2
σ_{hh}^2
b
Panoche soil
σ_a^2=0.0 cm^{-2}
σ_f^2=2.48
σ_q^2=0.0 cm^2/h^2
c
Panoche soil
α=0.0294 cm^{-1}
K$_s$=5.76 cm/h
q (cm/h)
c
Panoche soil
σ_a^2=0.0 cm^{-2}
σ_f^2=2.48
σ_q^2=0.0 cm^2/h^2
σ_q^2 (cm^2/h^2)

Figure 9

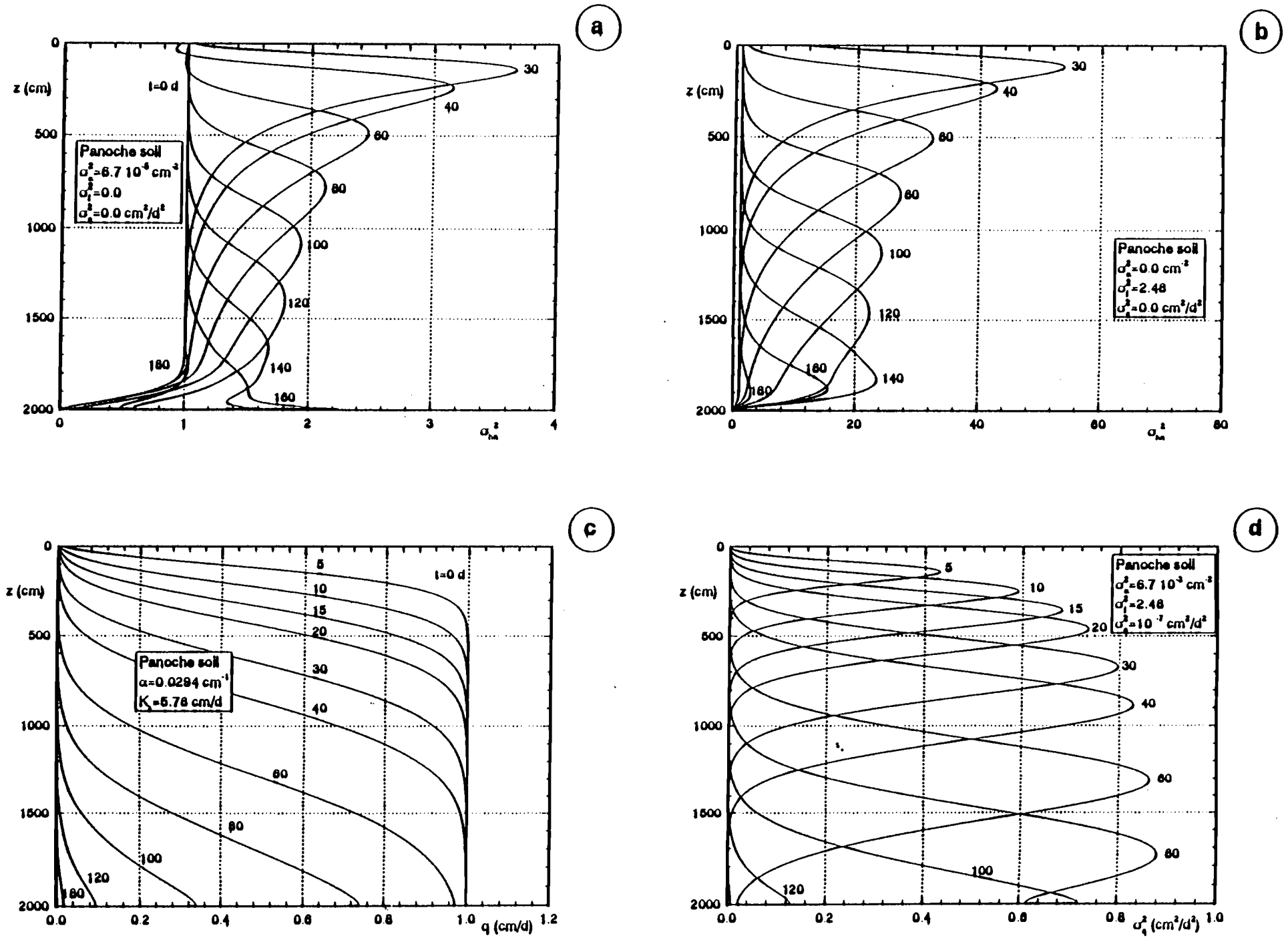
a
z (cm)
t=0 d
30
40
60
80
100
120
140
160
180
Panoche soil
σ_s^2=6.7 10^{-6} cm^{-2}
σ_f^2=0.0
σ_q^2=0.0 cm^2/d^2
σ_{hs}^2
b
z (cm)
30
40
60
80
100
120
140
160
180
Panoche soil
σ_s^2=0.0 cm^{-2}
σ_f^2=2.48
σ_q^2=0.0 cm^2/d^2
σ_{hs}^2
c
z (cm)
t=0 d
5
10
15
20
30
40
60
80
100
120
180
Panoche soil
α=0.0294 cm^{-1}
K$_s$=5.78 cm/d
q (cm/d)
d
z (cm)
5
10
15
20
30
40
60
80
100
120
Panoche soil
σ_s^2=6.7 10^{-3} cm^{-2}
σ_f^2=2.48
σ_q^2=10^{-7} cm^2/d^2
σ_q^2 (cm^2/d^2)

Figure 10

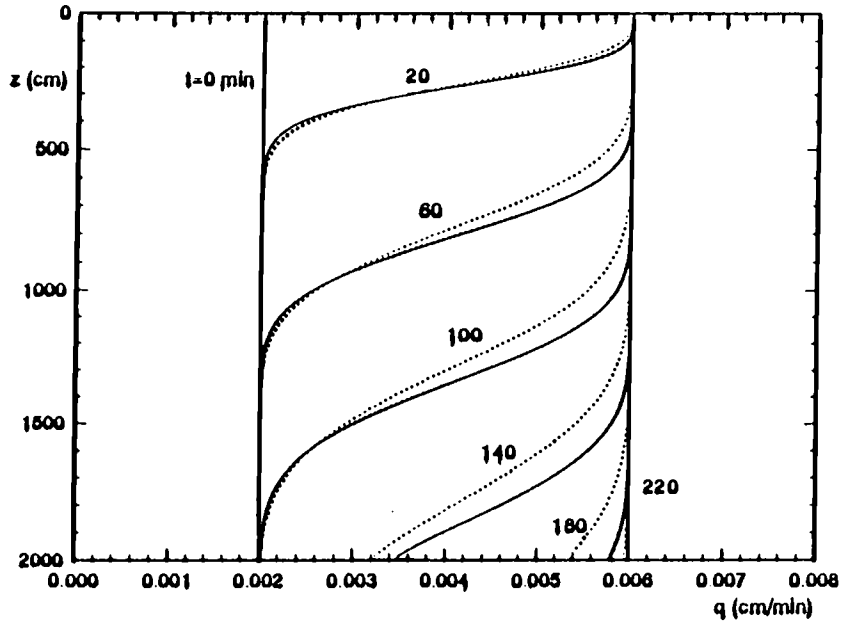
z (cm)
t=0 min
20
60
100
140
220
180
q (cm/min)

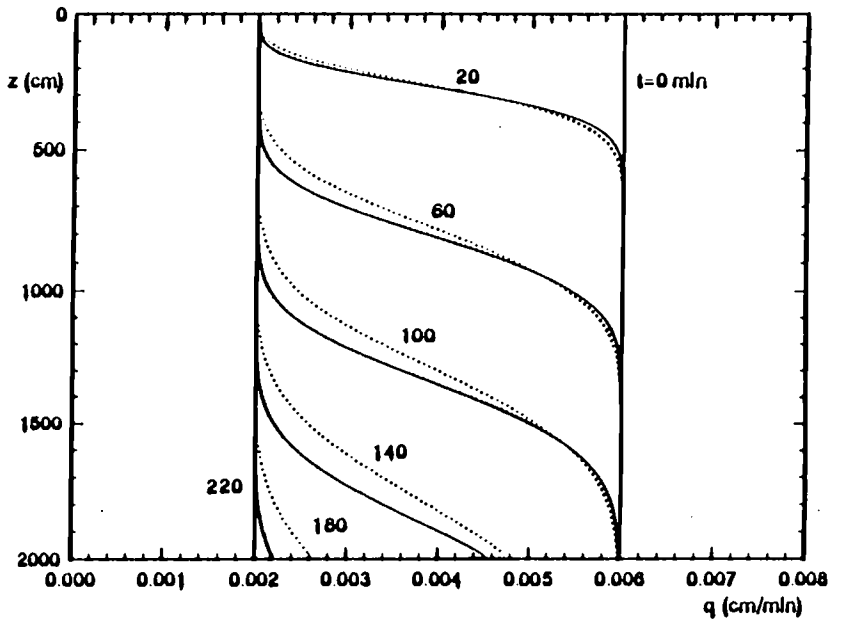
z (cm)
20
t=0 min
60
100
140
220
180
q (cm/min)

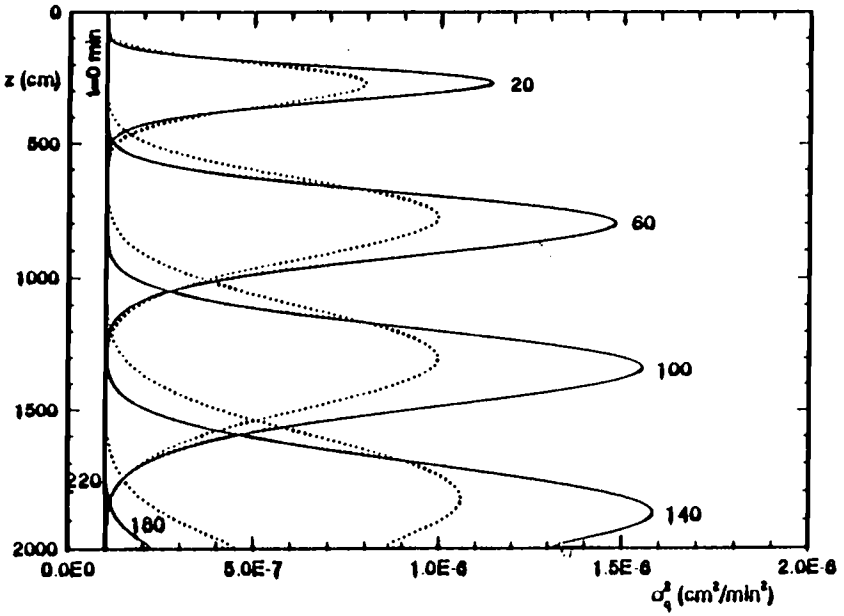
z (cm)
t=0 min
20
60
100
220
140
180
σ²q (cm²/min²)

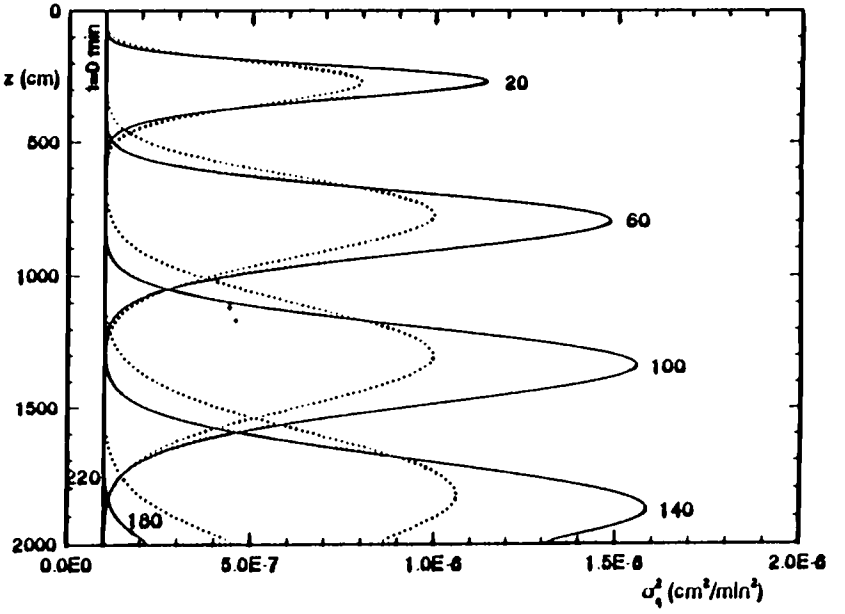
z (cm)
t=0 min
20
60
100
220
140
180
σ²q (cm²/min²)

Figure 11